Computational Materials Science 154 (2018) 365–370

Contents lists available at ScienceDirect

Computational Materials Science

journal homepage: www.elsevier.com/locate/commatsci

First-principle investigation of pressure and temperature influence on structural, mechanical and thermodynamic properties of Ti_3AC_2 (A = Al and Si)

Yuhong Zhao[a,*], Shijie Deng[a], Hu Liu[b,c], Jiaoxia Zhang[b,d], Zhanhu Guo[b], Hua Hou[a]

[a] College of Materials Science and Engineering, North University of China, Taiyuan 030051, China
[b] Integrated Composites Laboratory, Department of Chemical & Biomolecular Engineering, University of Tennessee, Knoxville, TN 37934, USA
[c] National Engineering Research Center for Advanced Polymer Processing Technology, Zhengzhou University, Zhengzhou 450002, China
[d] School of Material Science and Engineering, Jiangsu University of Science and Technology, Zhenjiang, Jiangsu 212003, China

ARTICLE INFO

Keywords:
Ti_3AlC_2 and Ti_3SiC_2
First principle
Mechanical properties
Thermodynamic properties

ABSTRACT

The mechanical and thermodynamic properties of Ti_3AlC_2 and Ti_3SiC_2 have been investigated by the first principles. The structure is briefly discussed, the compressibility of Ti_3SiC_2 is better than Ti_3AlC_2. Its mechanical stability is confirmed by the elastic constant, and the results show that the pressure can enhance the resistance to the deformation. In addition, the ductility is also improved with the pressure increasing. The elastic anisotropy is enhanced with increasing the pressure. Finally, the temperature and pressure dependences of thermodynamic properties of Ti_3AlC_2 and Ti_3SiC_2 are evaluated by the quasi-harmonic Debye approximation theory, and analyzed the effect of pressure and temperature on the Debye temperature, bulk modulus, heat capacity and the thermal expansion coefficient. The Debye temperature and bulk modulus decrease with increasing the temperature but increase with increasing the pressure. The temperature and pressure have opposite influences on the heat capacity, moreover, the ability of Ti_3AlC_2 to absorb or release heat is stronger than that of Ti_3SiC_2.

1. Introduction

The $M_{n+1}AX_n$ phases, where M is an early transition metal, A is an A-group element, and X is either C or N [1–5], have attracted more and more attention due to their uniquely combined properties of both ceramics and metals. Similar to ceramics, they are elastically rigid, lightweight and maintain their strengths to high temperature. Like metals, they are thermally plastic at high temperature and most readily machinable, which makes them potentially interesting for technological applications [6–8], including high-temperature structural applications [8], electrode brush materials, chemical anticorrosive materials and high-temperature heating materials [9–11].

Over the last few years, a concerted effort has been made to investigate the properties of the MAX phase. For example, Whittle et al. [9] studied the radiation tolerance of Ti_3AlC_2 and Ti_3SiC_2. Drouelle et al. [10] concluded the deformation mechanisms of Ti_3AlC_2 by the high temperature tensile creep experiments. The electronic and structural properties of the layered ternary carbide Ti_3AlC_2 were evaluated by Zhou et al. [11], they analyzed the band structure and Fermi level and revealed an electronic conductor of the Ti_3AlC_2. Wang et al. [12] examined the properties of vacancies in Ti_3AlC_2 and Ti_3SiC_2 and got the effective results of, they found that an A-group element mono-vacancy was more easily formed in Ti_3AlC_2, the vacancies tended to disperse in Ti_3SiC_2 but aggregate in Ti_3AlC_2. P. Finkel et al. [13] measured the low temperature dependence of the elastic properties including Young's shear modulus and they investigated the Debye temperature. Low temperature heat capacity of Ti_3SiC_2 was calculated by Ho et al. [14,15]. However there are little research on the effects of the temperature and pressure on the Ti_3AlC_2 and Ti_3SiC_2.

In this paper, we concentrated on exploring the effects of Ti_3AlC_2 and Ti_3SiC_2 under the pressure ranging from 0 to 50 GPa based on the first principle and calculating the bulk modulus, Debye temperature, heat capacity and the thermal expansion coefficient at temperature ranging from 0 to 1000 K to investigate the thermodynamic properties by the quasi-harmonic Debye approximation theory.

2. Computational methods

The first principle calculations have been performed based on the density functional theory (DFT) [16] and the Cambridge Serial Total

* Corresponding author.
E-mail address: zhaoyuhong@nuc.edu.cn (Y. Zhao).

https://doi.org/10.1016/j.commatsci.2018.07.007
Received 10 June 2018; Received in revised form 3 July 2018; Accepted 5 July 2018

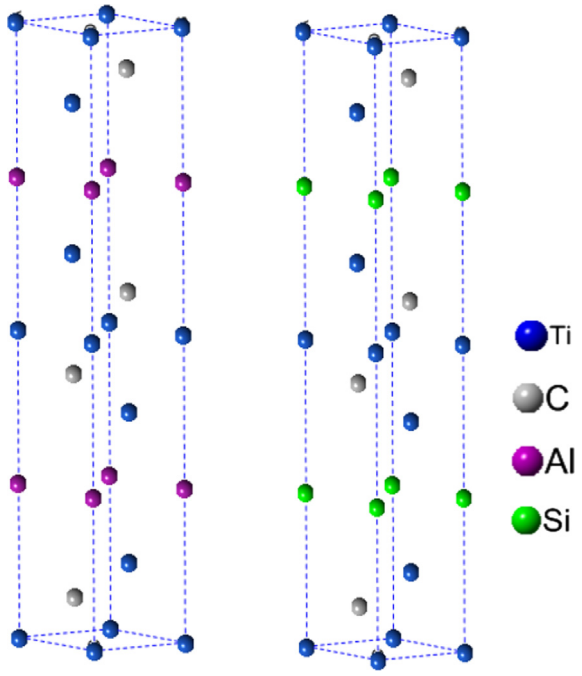

Fig. 1. The crystal structure of Ti_3AlC_2 and Ti_3SiC_2.

Energy Package (CASTEP) [17], in which a plane wave ultra-soft pseudopotential [18] is used. The generalized gradient approximation (GGA) with Perdew-Burke-Ernzerhof (PBE) approach [19] is performed to represent the exchange-correlation function. By convergence, the plane-wave basis set cutoff was set as 440 eV and the *k*-point mesh to 13 × 13 × 2 for all cases, the energy was converged to better than 5.0×10^{-6} eV/atom, whereas the maximum force and stress had been determined as 0.01 eV/Å and 0.02 GPa, respectively. The maximum displacement was set as 5.0×10^{-4} Å.

The Ti_3AlC_2 and Ti_3SiC_2 are hexagonal structures, as shown in Fig. 1. Which can be regarded as alternating stacks of two layers, the space group is $P6_3/mmc$. The Al or Si atoms are located in the (0, 0, 1/4) positions, the Ti atoms are located in at (0, 0, 0) and (2/3, 1/3, z_{Ti}) and the C atoms are located at (1/3, 2/3, z_c) [20,21].

3. Results and discussions

3.1. Structural properties

The relative changes of equilibrium volume and lattice parameters at various pressures ranging from 0 to 50 GPa with a step of 10 GPa are shown in Fig. 2, where V_0 and a_0 are the zero pressure equilibrium structural parameters. It is easy to see that the ratio of V/V_0 of Ti_3AC_2 (X = Al and Si) was reduced by 18.7% and 16.9%, respectively. Therefore, the compressibility of the system is strong. The volume change ratio with pressure gradually decreases as the order of Ti_3AlC_2 > Ti_3SiC_2. As for the Ti_3AC_2, the volume was reduced with increasing the internal pressure. At high pressure, the V/V_0 curves become gentle, since the distance change in the atoms gets smaller and thus the mutual repulsion of the atoms gets stronger, which leads to the difficulty of compression in crystal.

3.2. Mechanical properties

The elastic constants (C_{ij}), bulk modulus (B) and shear modulus (G) were calculated and listed in Table 1. The available theoretical date under different pressures was included for comparison. Because the Ti_3AC_2 is a hexagonal crystal, which has six different independent elastic constants (C_{11}, C_{12}, C_{13}, C_{33}, C_{44} and C_{66}), but only five of them

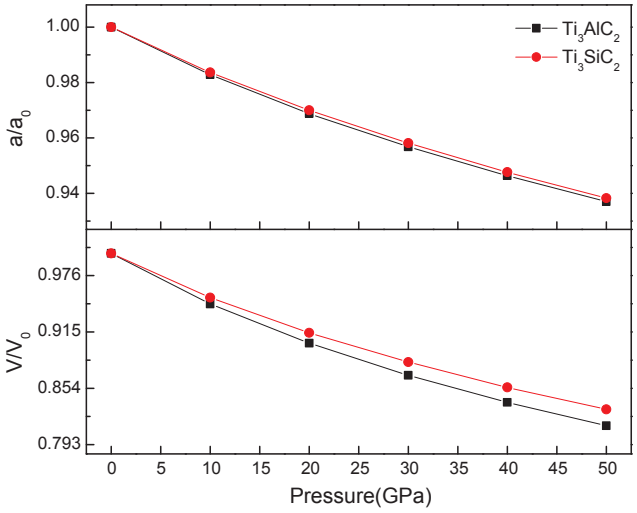

Fig. 2. The normalized lattice parameters a/a_0 and volume V/V_0 of Ti_3AlC_2 and Ti_3SiC_2 at various pressures.

are independent since $C_{66} = (C_{11} - C_{12})/2$ [22], thus only five independent elastic constants were listed. The mechanical stability of system can be judged by the Born stability criteria [23]:

$$C_{11} > 0,\ C_{11} - C_{12} > 0,\ C_{44} > 0,\ C_{66} > 0,\ (C_{11} + C_{12})C_{33} - 2C_{13}^2 > 0 \quad (1)$$

It is obviously to note that the elastic constants in the pressure range 0–50 GPa satisfy Eq. (1), which indicates that they are mechanically stable under compression and the value of C_{ij} goes up linearly with increasing the pressure, besides the C_{11} and C_{33} increase more rapidly than others.

As for the bulk modulus and shear modulus, these quantities are given by Eqs. (2)(7) [24–26]:

$$B_V = \frac{2(C_{11} + C_{12}) + C_{33} + 4C_{13}}{9} \quad (2)$$

$$B_R = \frac{(C_{11} + C_{12})C_{33} - 2C_{13}^2}{C_{11} + C_{12} + 2C_{33} - 4C_{13}} \quad (3)$$

$$B_H = \frac{B_V + B_R}{2} \quad (4)$$

$$G_V = \frac{C_{11} + C_{12} + 2C_{33} - 4C_{13} + 12C_{55} + 12C_{66}}{30} \quad (5)$$

$$G_R = \frac{5}{2} \frac{[(C_{11} + C_{12})C_{33} - 2C_{13}^2]C_{55}C_{66}}{3B_V C_{55}C_{66} + [(C_{11} + C_{12})C_{33} - 2C_{13}^2](C_{55} + C_{66})} \quad (6)$$

$$G_H = \frac{G_V + G_R}{2} \quad (7)$$

where bulk modulus B_B, B_R and B_H represent the maximum, minimum and average value, respectively, and the shear modulus G_B, G_R and G_H also represent the maximum, minimum and average value.

The values of B and G play an important role on the mechanical properties of materials. The value of the B and G increases linearly at various pressures ranging from 0 to 50 GPa with a step of 10 GPa, the bulk modulus is usually assumed to be a measure of resistance to volume change by applied pressure, which implies that pressure can improve the resistance to volume deformation. As for shear modulus and Young's modulus, the trend is similarly to the bulk modulus. The Young's modulus is used to provide a measure of the capability of resisting the tension and pressure in the range of elastic deformation [27]. Generally speaking, the larger the Young's modulus is, the harder it is to deform the material. The value of B, G and E of Ti_3SiC_2 is found to be higher than that of Ti_3AlC_2, the effect of resisting the deformation for the Ti_3SiC_2 is better than Ti_3AlC_2. Therefore, the change of external

Table 1
Variations of elastic constants (GPa) of Ti_3AC_2 with pressure.

Ti_3AC_2	Pressure	C_{11}	C_{12}	C_{13}	C_{33}	C_{44}	B_V	B_R	B_H	G_v	G_R	G_H	E	B/G	A
Ti_3AiC_2	0	356.8	70.2	69.2	329.7	139.8	162.2	162.0	162.1	140.2	140.1	140.2	326.4	1.16	0.99
	Cal.[30]	361.0	75.0	70.0	299.0	124.0	–	–	160.0	–	–	131.0	334.0	–	–
	10	414.7	96.3	99.9	359.5	145.9	197.9	197.2	197.6	149.7	149.1	149.4	358.0	1.32	0.99
	20	472.0	125.2	134.1	407.7	174.2	237.6	236.9	237.2	168.2	167.3	167.8	407.3	1.41	1.08
	30	519.0	153.3	166.4	461.9	189.2	274.7	274.2	274.4	179.8	178.8	179.3	441.7	1.53	1.11
	40	564.1	174.7	196.6	511.8	204.8	308.4	308.2	308.3	192.3	190.9	191.6	476.2	1.61	1.18
	50	604.7	199.9	225.7	551.5	219.2	340.4	340.2	340.3	202.1	200.2	201.1	504.1	1.69	1.20
Ti_3SiC_2	0	370.4	84.6	99.2	361.5	164.1	185.4	185.3	185.3	148.9	147.7	148.3	351.1	1.25	1.23
	Exp.[12]	–	–	–	–	–	–	–	187.0	–	–	142.0	339.0	–	–
	10	428.0	106.6	138.3	426.0	197.2	227.6	227.4	227.5	170.9	167.8	169.4	407.1	1.34	1.37
	20	480.3	132.9	170.7	478.3	219.4	265.3	265.0	265.1	186.8	182.5	184.6	449.6	1.44	1.42
	30	529.4	157.9	204.4	525.2	243.8	301.9	301.5	301.7	202.5	196.1	199.3	489.9	1.51	1.51
	40	574.8	185.4	237.4	574.9	265.9	338.3	337.7	338.0	216.2	207.9	212.0	526.1	1.59	1.58
	50	617.0	209.7	269.6	620.7	286.0	372.5	371.6	372.0	228.8	218.4	223.6	558.9	1.66	1.64

pressure has the bigger impact on Ti_3SiC_2.

The ductility and brittleness can be judged according to Pugh's criterion (B/G) [28]. The B/G ratio separates ductile (> 1.75) and brittle (> 1.75) materials. The value of B/G increases linearly with the increase of the applied pressure, which indicates that the ability to resist deformation has been improved. The bulk moduli reflect the resistance to the bond-length change, and the shear modulus directly corresponds to the bond-angle change with the applied stress. It is believed that the material is ductile if it has a larger bulk modulus and smaller shear modulus [29]. Obviously, the growth rate of the bulk modulus is larger than that of the shear modulus and the ductility is enhanced. Besides, the Ti_3AlC_2 and Ti_3SiC_2 behave in a brittle manner at 0 GPa, and the ductility is also improved with the pressure increasing, the value of B/G is increased near to 1.75.

For hexagonal crystals, the elastic anisotropy (A), which is related the micro cracks and has an essential effect on the nanoscale precursor textures in materials, plays a vital role in materials science, can be obtained by Eq. (8) [31]:

$$A = \frac{4C_{44}}{C_{11} + C_{33} - 2C_{13}} \tag{8}$$

Our calculation results are summarized in Table 1. It is easy to find that all of the values are not equal to 1, this indicates that the materials are elastic anisotropy. But the change of elastic anisotropy is not obvious for Ti_3AlC_2. The 3D Young's modulus surface can be obtained using the equation [32]:

$$\frac{1}{E} = S_{11}(l_1^4 + l_2^4 + 2l_1^2 l_2^2) + S_{33} l_3^4 + (S_{44} + 2S_{13})(l_1^2 + l_2^2) l_3^2 \tag{9}$$

where S_{ij} represents the elastic compliance coefficient and l_i represents direction cosine.

Fig. 3 plots the 3D Young's modulus surface [33] of Ti_3AlC_2 (a, b, c) and Ti_3SiC_2 (d, e, f) at 0, 25 and 50 GPa, respectively. The depth of the color reflects the magnitude of Young's modulus. It can illuminate that the Ti_3AC_2 has elastic anisotropy, thus the shape begins to deviate from sphere with increasing the pressure, and the color begins to darken, it indicates that the Young' modulus increases with increasing the pressure. The results agree well with the previous calculations as illustrated in Table 1. The Young's modulus of Ti_3AlC_2 and Ti_3SiC_2 are 326.4 Gpa and 351.1 GPa when the pressure is 0 GPa. And when the pressure is 50 GPa, the Young's modulus of Ti_3AlC_2 and Ti_3SiC_2 are 504.1 GPa and 558.9 GPa, respectively. The effect of the elastic anisotropy on pressure of Ti_3SiC_2 is bigger than Ti_3AlC_2. Furthermore, according to the deviation degree of spherical shape, the anisotropy of Ti_3SiC_2 is bigger than Ti_3AlC_2.

3.3. Thermodynamic properties

The thermodynamic properties are evaluated in the temperature ranging from 0 to 1000 K and the pressure is up to 50 GPa, where the quasi-harmonic Debye approximation theory [34,35] remains valid. The Debye temperature, bulk modulus, heat capacity and the thermal expansion coefficient are investigated to disclose the thermodynamic properties of Ti_3AlC_2 and Ti_3SiC_2.

The calculated Debye temperature is displayed in Fig. 4. The Debye temperature of materials plays an important role in many physical properties of solids, such as specific heat, thermal expansion [36]. The Debye temperatures of Ti_3AlC_2 as well as Ti_3SiC_2 are 741.26 and 796.06 K at room temperature, which is consistent with the calculated Debye temperatures by P. Finkel et al. [37] (758 K and 780 K for Ti_3AlC_2 and Ti_3SiC_2 respectively which were calculated by using a phase sensitive pulse-echo ultrasonic technique). Furthermore, it can be seen that the Debye temperature decreases with increasing the temperature, but increases with increasing the applied pressure, and the effect of pressure is larger than that of temperature.

Fig. 5 shows the temperature and pressure dependence of bulk modulus of Ti_3AC_2. The trend of bulk modulus is similar to the Debye temperature. The bulk modulus decreases linearly with increasing the temperature but increases with increasing the pressure at a constant temperature, indicating that increasing pressure or decreasing temperature can improve the materials hardness.

The variation of heat capacity C_V and C_p as a function of temperature is depicted in Fig. 6(a) and (b). Both C_V and C_p are observed to increase with increasing the temperature when the temperature is below 300 K. However, the C_V and C_p increase slowly at high temperature, the results show that the interactions between ions in Ti_3AC_2 have a great effect on the heat capacity at low temperature. In addition, the curve of C_V comes to a line at high temperature since the C_V obeys the Dulong-Petit limit. It is easy to see that the temperature and pressure have opposite influences on the heat capacity and the effect of temperature is more significant than the pressure when the pressure is less than 300 K. The C_V and C_p from high to low are Ti_3AlC_2 and Ti_3SiC_2, this indicates that the ability of Ti_3AlC_2 to absorb or release heat is stronger than that of Ti_3SiC_2 [38].

Finally, the thermal expansion coefficient is plotted in Fig. 7. The effect of pressure is not well when the temperature is in the range of 0–300 K, and the curves become gentle with increasing the temperature, which indicates that the effect of temperature mainly occurs at low temperatures. The value of thermal expansion coefficient decreases with increasing the pressure at a given temperature.

4. Conclusions

The effects of pressure and temperature on the mechanical and

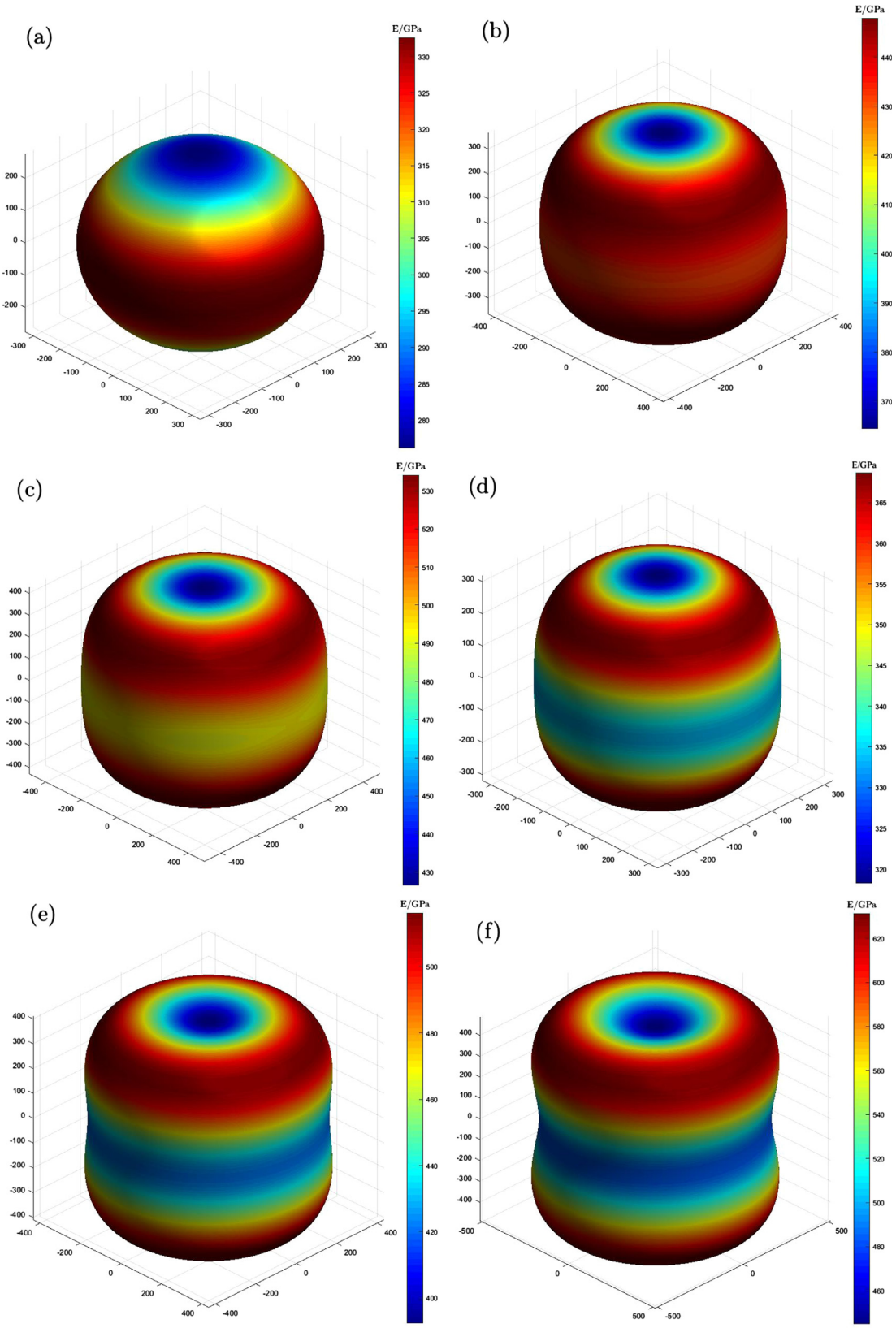

Fig. 3. The 3D Young's modulus E surface of Ti_3AlC_2 and Ti_3SiC_2 at various pressure.

thermodynamic properties of Ti_3AlC_2 and Ti_3SiC_2 were calculated by using first principles. The volume ratio and lattice parameters of Ti_3AlC_2 and Ti_3SiC_2 decrease with increasing the internal pressure, and the compressibility of Ti_3AlC_2 is better than that of Ti_3SiC_2. The pressure can improve the resistance to deformation. The effect of pressure on the Ti_3SiC_2 is obvious, and the ductility is also improved with the pressure increasing. Both the Ti_3AlC_2 and Ti_3SiC_2 are elastic anisotropy by the calculated elastic anisotropy. The thermodynamic

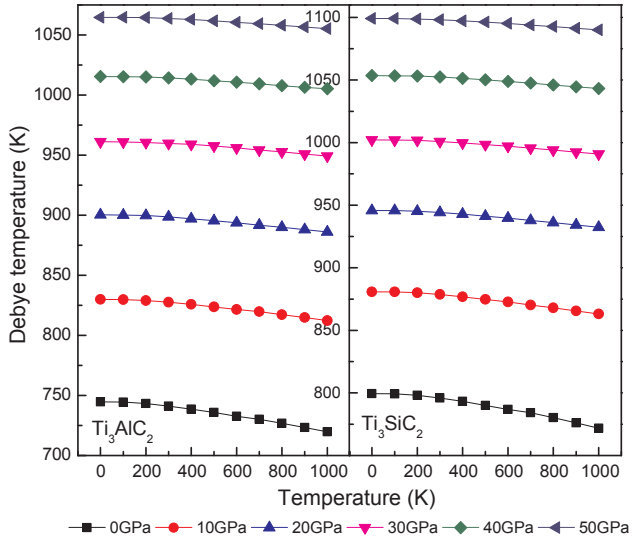

Fig. 4. The pressure and temperature dependence of Debye temperature for Ti_3AlC_2 and Ti_3SiC_2.

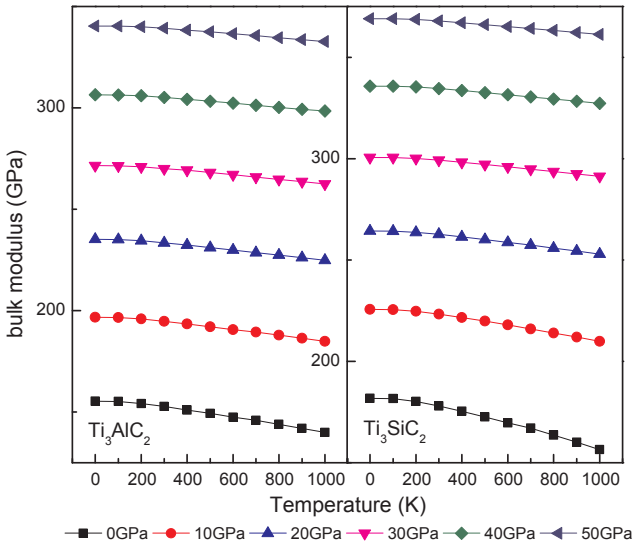

Fig. 5. The pressure and temperature dependence of bulk modulus for Ti_3AlC_2 and Ti_3SiC_2.

properties are evaluated based on the quasi-harmonic Debye approximation theory, both Debye temperature and bulk modulus decrease with increasing the temperature but increase with increasing the pressure, and the temperature and pressure have opposite influences on the heat capacity, moreover, the ability of Ti_3AlC_2 to absorb or release heat is stronger than that of Ti_3SiC_2. The reported theoretical method is also applicable to other systems such as ceramic, metal, carbon, polymer and their composites [39–56]. For ceramic, the mechanical properties and electronic properties can be analyzed. Meanwhile, the interface performance of the composites can be predicted by using this simulation method as well.

Author contributions

Yuhong Zhao, Shijie Deng, and Hua Hou have carried out the simulation work.

Hu Liu, Jiaoxia Zhang, and Zhanhu Guo have carried out the parameter selection and methodology discussion.

Yuyong Zhao and Hua Hou contributed to the funding acquisition.

All authors have taken part in the draft, review & editing of the

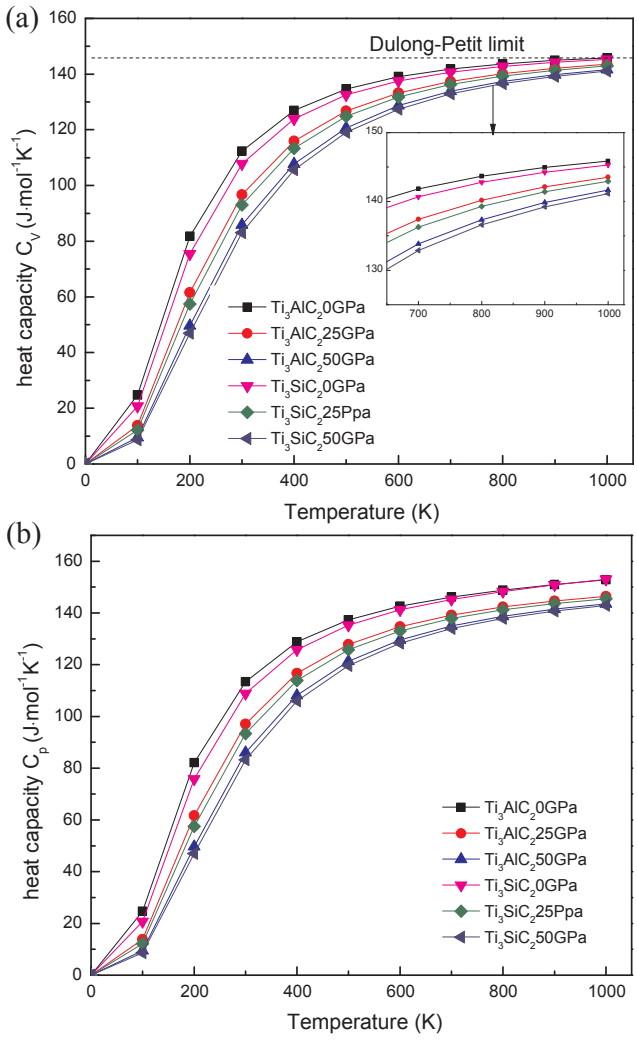

Fig. 6. The pressure and temperature dependence of heat capacity C_V (a) and C_p (b) for Ti_3AlC_2 and Ti_3SiC_2.

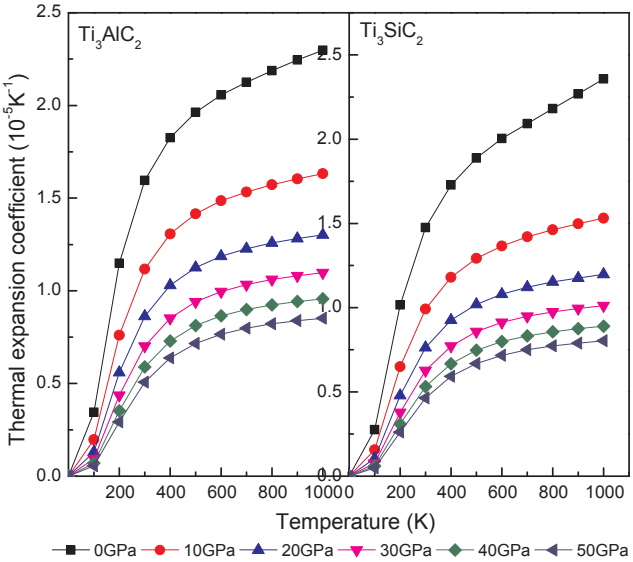

Fig. 7. The pressure and temperature dependence of thermal expansion coefficient for Ti_3AlC_2 and Ti_3SiC_2.

paper.

Acknowledgements

This work is supported by the National Natural Foundation of China (Nos. 51774254, 51774253, 51701187, U1610123, 51674226,51574207, 5157420), The Science and Technology Major Project of Shanxi Province (No.MC2016-06).

Data Availability

The data will be provided upon the request after consulting with the intelligent office of the universities.

References

[1] M.W. Barsoum, The MAX phases: a new class of solids, Prog. Solid State Chem. 28 (2000) 201–281.
[2] M.W. Barsoum, T. El-Raghy, T. The MAX, Phases: unique new carbide and nitride materials: ternary ceramics turn out to be surprisingly soft and machinable, yet also heat-tolerant, strong and lightweight, Am. Sci. 89 (2001) 334–343.
[3] S. Aryal, R. Sakidja, L. Ouyang, W.Y. Ching, Elastic and electronic properties of $Ti_2Al(C_xN_{1-x})$ solid solutions, Eur. Ceram. Soc. 35 (2015) 3219–3227.
[4] V.J. Keast, S. Harris, D.K. Smith, Prediction of the stability of the $M_{n+1}AX_n$, phases from first principles, Phys. Rev. B 21 (2009) 308–310.
[5] W. Ching, Y. Mo, S. Aryal, P. Rulis, Intrinsic mechanical properties of 20 MAX-phase compounds, Am. Ceram. Soc. 96 (2013) 2292–2297.
[6] N. Atazadeh, M.S. Heydari, H.R. Baharvandi, N. Ehsani, Reviewing the effects of different additives on the synthesis of the Ti_3SiC_2, MAX phase by mechanical alloying technique, Int. J. Refract. Met. Hard Mater. 61 (2016) 67–78.
[7] M. Hopfeld, R. Grieseler, A. Vogel, H. Romanus, P. Schaaf, Tribological behavior of selected $M_{n+1}AX_n$ phase thin films on silicon substrates, Surf. Coat. Int. 257 (2014) 286–294.
[8] G.M. Song, S.B. Li, C.X. Zhao, W.G. Sloof, S. V D Zwaag, Y.T. Pei, J.T. M Hosson, Ultra-high temperature ablation behavior of Ti_2AlC ceramics under an oxyacetylene flame, Eur. Ceram. Soc. 31 (2011) 855–862.
[9] K.R. Whittle, M.G. Blackford, R.D. Aughterson, S. Moricca, G.R. Lumpkin, D.P. Riley, N.J. Zaluzec, Radiation tolerance of $M_{n+1}AX_n$, phases, Ti_3AlC_2, and Ti_3SiC_2, Acta Mater. 58 (2010) 4362–4368.
[10] E. Drouelle, A. Joulain, J. Cormier, V. Gautheir-Brunet, P. Villechaise, S. Dubois, P. Sallot, Deformation mechanisms during high temperature tensile creep of Ti3AlC2, MAX phase, J. Alloys. Compd. 693 (2017) 622–630.
[11] Y.C. Zhou, X.H. Wang, Z.M. Sun, S.Q. Chen, Electronic and structural properties of layered ternary carbide Ti_3AlC_2, J. Mater. Chem. 11 (2001) 2335–2339.
[12] H. Wang, H. Han, G. Yin, C.Y. Wang, Y.Y. Houo, J. Tang, J.X. Dai, C.L. Ren, W. Zhang, P. Huai, First-principles study of vacancies in Ti_3SiC_2 and Ti_3AlC_2, Materials 10 (2017) 103.
[13] P. Finkel, M.W. Barsoum, T. Elraghy, Low temperature dependence of the elastic properties of Ti_3SiC_5, J. Appl. Phys. 85 (1999) 7123–7126.
[14] J.C. Ho, H.H. Hamdeh, M.W. Barsoum, T. EI-Raghy, Low temperature heat capacities of $Ti_3Al_{1.1}C_{1.8}$, Ti_4AlN_3, and Ti_3SiC_2, J. Appl. Phys. 86 (1999) 3609–3611.
[15] J.C. Ho, H.H. Hamdeh, M.W. Barsoum, T. Elraghy, Low temperature heat capacity of Ti_3SiC_2, J. Appl. Phys. 85 (1999) 7970–7971.
[16] J.P. Perdew, Density functional approximation for the correlation energy of the Inhomogeneous electron gas, Phys. Rev. B 33 (1986) 8822.
[17] M. Segall, P.J. Lindan, M. Probert, C. Pickard, P. Hasnip, S. Clark, M. Payne, First-principles simulation: ideas, illustrations and the CASTEP code, Phys. Condens. Matter. 14 (2002) 2717.
[18] D. Vanderbilt, Soft self-consistent pseudopotentials in a generalized eigenvalue formalism, Phys. Rev. B 41 (1990) 7892.
[19] J.P. Perdew, K. Burke, M. Ernzerhof, Generalized gradient approximation made simple, Phys. Rev. Lett. 77 (1996) 3865–3868.
[20] N.I. Medvedeva, A.J. Freeman, Cleavage fracture in Ti_3SiC_2 from first-principles, Scr. Mater. 58 (2008) 671–674.
[21] R.X. Jing, X.W. Chen, F.Y. Teng, Y.K. Shu, M.X. Jian, G.Y. Yu, Theoretical investigation on helium incorporation in Ti_3AlC_2, Nucl. Instrum. Meth. Phys. Res. Sect. B 304 (2013) 27–31.
[22] H. Li, G. Sun, J. Deng, W. Zhang, L. Xu, W. Jiang, Y. Feng, K. Li, Phonon and electronic properties of Ti_2SiC from first-principles calculations, Solid State Commun. 204 (2015) 37–40.
[23] S.J. Deng, Y.H. Zhao, H. Hou, Z.Q. Wen, P.D. Han, Structural, mechanical and thermodynamic properties of Ti_2AlX (X= C, N) at high pressure, Acta Phys. Sinica 66 (2017) 146101.
[24] R. Hill, Proc, the elastic behavior of a crystalline aggregate, Phys. Soc. A 65 (1952) 349–354.
[25] W. Voigt, Leipzig: Teubner (1928) 95–100.
[26] A. Reuss, Berechnung der fliessgrenze von mischkristallen auf grund der plastizitätsbedingung für einkristalle, Z. Angew. Math. Mech. 9 (1929) 49–58.
[27] Y. Tu, Y. Wang, First-principles study of the elastic properties of [formula omitted] and [formula omitted] alloys, Solid State Commun. 151 (2011) 238.
[28] L. Qi, Y.C. Jin, Y.H. Zhao, X.M. Yang, H. Zhao, P.D. Han, The structural, elastic, electronic properties and debye temperature of Ni_3Mo under pressure from first-principles, J. Alloys Compd. 621 (2015) 383–388.
[29] Z.Q. Wen, Y.H. Zhao, H. Hou, J.Z. Tian, P.D. Han, First-principles studied Ni-Al intermetallic compounds under various temperature and pressure, Superlatt. Microstruct. 103 (2016) 9–18.
[30] J. Wang, Y. Zhou, Dependence of elastic stiffness on electronic band structure of nanolaminate M_2AlC, (M = Ti, V, Nb, and Cr) ceramics, Phys. rev. B 69 (2004) 1681–1685.
[31] Z. Sun, S. Li, R. Ahuja, J.M. Schneider, Calculated elastic properties of M_2AlC (M=Ti, V, Cr, Nb and Ta), Solid State Chem. 129 (2004) 589–592.
[32] J.F. Nye, Physical, Properties of Crystal: their Represent by Tensors and Matrices, Oxford university Press, New york, 1985.
[33] A. Marmier, Z.A.D. Lethbridge, R.I. Walton, W. SmithC, S.C. Parker, K.E. Evans, ElAM: a computer program for the analysis and representation of anisotropic elastic properties, Comput. Phys. Commun. 181 (2010) 2102–2115.
[34] M.A. Blanco, E. Francisco, V. Luaña, Comput, GIBBS: isothermal-isobaric thermodynamics of solids from energy curves using a quasi-harmonic Debye model, Phys. Commun. 158 (2004) 57–72.
[35] A. Otero-De-La-Roza, D. Abbasi-Pérez, V. Luaña, GIBBS2: a new version of the quasiharmonic model code. II. Models for solid-state thermodynamics, features and implementation, Comput. Phys. Commun. 182 (2011) 2232–2248.
[36] M. Pang, Y. Zhan, H. Wang, W. Jiang, Y. Du, Ab initio study of $AlCu_2M$ (M = Sc, Ti and Cr) ternary compounds under pressures, Comput. Mater. Sci. 50 (2011) 2930–2937.
[37] P. Finkel, M.W. Barsoum, T. Elraghy, Low temperature dependencies of the elastic properties of Ti_4AlN_3, $Ti_3Al_{1.1}C_{1.8}$, and Ti_3SiC_2, J. Appl. Phys. 57 (2000) 1701–1703.
[38] Z.Q. Wen, Y.H. Zhao, H. Hou, B. Wang, P.D. Han, The mechanical and thermodynamic properties of Heusler compounds Ni_2XAl (X = Sc, Ti, V) under pressure and temperature: a first-principles study, Mater. Des. 114 (2017) 398–403.
[39] Z. Zhao, R. Guan, J. Zhang, Z. Zhao, P. Bai, Effects of process parameters of semi-solid stirring on microstructure of Mg-3Sn-1Mn-3SiC (wt%) strip processed by rheo-rolling, Acta Metall. Sin. (Engl. Lett.) 30 (2017) 66–72.
[40] F. Liu, Z. Xu, Z. Wang, M. Dong, J. Deng, Q. Yao, H. Zhou, Y. Ma, J. Zhang, N. Wang, Z. Guo, Structures and mechanical properties of Nb-Mo-Co(Ru) solid solutions for hydrogen permeation, J. Alloys Compd. 756 (2018) 26–32.
[41] H. Du, Y. An, X. Zhang, Y. Wei, L. Hou, B. Liu, H. Liu, J. Zhang, N. Wang, A. Umar, Z. Guo, Hydroxyapatite (HA) modified nanocoating enhancement on AZ31 Mg alloy by combined surface mechanical attrition treatment and electrochemical deposition approach, J. Nanosci. Nanotechnol. (2018), https://doi.org/10.1166/jnn.2018.15746 (in press).
[42] H. Du, Y. An, Y. Wei, L. Hou, et al., Nickel powders modified nanocoating strengthened iron plates by surface mechanical attrition alloy and heat treatment, Sci. Adv. Mater. 10 (2018) 1063–1072.
[43] Q. Luo, H. Ma, Q. Hou, Y. Li, et al., All-carbon-electrode-based endurable flexible perovskite solar cells, Adv. Funct. Mater. 28 (2018) 1706777.
[44] J. Lin, X. Chen, C. Chen, et al., Durably antibacterial and bacterially anti-adhesive cotton fabrics coated by cationic fluorinated polymers, ACS Appl. Mater. Interf. 10 (2018) 6124–6136.
[45] K. Sun, R. Fan, X. Zhang, et al., An overview of metamaterials and their achievements in wireless power transfer, J. Mater. Chem. C 6 (2018) 2925–2943.
[46] Z. Hu, Q. Shao, Y. Huang, L. Yu, D. Zhang, X. Xu, J. Lin, H. Liu, Z. Guo, Light triggered interfacial damage self-healing of poly(p- phenylene benzobisoxazole) fiber composites, Nanotechnology 29 (2018) 185602.
[47] Y. Zhang, M. Zhao, J. Zhang, et al., Excellent corrosion protection performance of epoxy composite coatings filled with silane functionalized silicon nitride, J. Polym. Res. 25 (2018) 130.
[48] H. Gu, H. Zhang, J. Lin, et al., Large negative giant magnetoresistance at room temperature and electrical transport in cobalt ferrite-polyaniline nanocomposites, Polymer 143 (2018) 324–330.
[49] C. Wang, B. Mo, Z. He, et al., Hydroxide ions transportation in polynorbornene anion exchange membrane, Polymer 138 (2018) 363–368.
[50] J. Zhao, L. Wu, C. Zhan, Q. Shao, Z. Guo, L. Zhang, Overview of polymer nanocomposites: computer simulation understanding of physical properties, Polymer 133 (2017) 272–287.
[51] C. Wang, B. Mo, Z. He, et al., Crosslinked norbornene copolymer anion exchange membrane for fuel cells, J. Membr. Sci. 556 (2018) 118–125.
[52] Z. Sun, et al., Experimental and simulation understanding of morphology controlled barium titanate nanoparticles under co-adsorption of surfactants, CrystEngComm 19 (2017) 3288–3298.
[53] T. Wu, Q. Shao, S. Ge, L. Bao, Q. Liu, The facile preparation of novel magnetic zirconia composites with the aid of carboxymethyl chitosan and their efficient removal of dye, RSC Adv. 6 (2016) 58020–58027.
[54] H. Liu, Y. Ding, B. Yang, Z. Liu, Q. Liu, X. Zhang, Colorimetric and ultrasensitive detection of H_2O_2 Based on Au/Co_3O_4-CeO_x nanocomposites with enhanced peroxidase-like performance, Sensor Actuat. B: Chem. 271 (2018) 336–345.
[55] X. Zhu, W. Chen, K. Wu, H. Li, M. Fu, Q. Liu, X. Zhang, Colorimetric sensor of H_2O_2 based on Co_3O_4-montmorillonite nanocomposites with the peroxidase activity, New J. Chem. 42 (2018) 1501–1509.
[56] Z. Hu, D. Zhang, L. Yu, Y. Huang, Light-triggered C_{60} release from a graphene/cyclodextrin nanoplatform for the protection of cytotoxicity induced by nitric oxide, J. Mater. Chem. B 6 (2018) 518–526.